

Power System Robust State Estimation As a Layer: A Novel End-to-end Learning Approach

Yibo Ding, *Student Member, IEEE*, Wenzhuo Shi, *Student Member, IEEE*,
 Mengzhao Duan, *Student Member, IEEE*, Yuhong Zhao, *Student Member, IEEE*,
 Jiaqi Ruan, *Member, IEEE*, Jian Zhao, *Member, IEEE*, and Zhao Xu, *Senior Member, IEEE*

Abstract—Serving as an essential prerequisite for modern power system operation, robust state estimation (RSE) could effectively resist noises and outliers in measurements. The emerging neural network (NN) based end-to-end (E2E) learning framework enables real-time application of RSE but cannot strictly enforce the physical constraints involved, potentially yielding solutions that are statistically accurate yet physically inconsistent. To bridge this gap, this work proposes a novel E2E learning based RSE framework, where the RSE problem is innovatively constructed as an explicit differentiable layer of NN for the first time, ensuring physics alignments with rigors. Also, the measurement weights are treated as learnable parameters of NN to enhance estimation robustness. A hybrid loss function is formulated to pursue accurate and physically consistent solutions. To realize the proposed NN structure, the original non-convex RSE problem is specially relaxed. Extensive numerical simulations have been carried out to demonstrate that the proposed framework can significantly improve the SE performance while fulfilling physical consistency on six testing systems, in comparisons to the classical E2E learning based approach and the physics-informed neural network (PINN) approach.

Index Terms—State estimation, end-to-end learning, robust regression, neural network

I. INTRODUCTION

THE ultimate goal of power system state estimation (PSSE) is to calculate state variables according to real-time measurements by minimizing the measurement errors, also called residuals, providing a snapshot of the grid's conditions for system operation and control. Traditionally, it is conducted after topology identification and observability checking, and followed by the processing of bad measurement data, namely the outliers [1]. Real-time measurements are often available from supervisory control and data acquisition (SCADA) systems in modern smart grids [2]. The measurement set typically comprises bus voltage magnitudes, nodal power injections, and branch power flows. The state variables to be estimated are the complex voltages, i.e., the voltage magnitudes and phase angles at all buses.

Conventionally, PSSE is formulated as a constrained optimization problem calculating the weighted least squares (WLS) of residuals under the Gaussian assumption of noises, solving by iterative approaches such as Newton-Raphson algorithm [3]. Nevertheless, the WLS-based estimator suffers from sensitivity in the presence of outliers originating from sensor

malfunctions or communication failures [4]. Outliers would therefore introduce a significant bias to the estimation results. Traditionally, the chi-square test is carried out to identify outliers, followed by the corresponding removal and repeated estimation [5]. To enhance the estimation robustness against outliers, research has shifted towards robust state estimation (RSE). One prominent RSE approach is to dynamically adjust the measurement weights [6] [7], which are assumed as constants in classic PSSE models [1]. To be specific, the weights are iteratively updated according to the residuals calculated in the repeated estimation [8] [9], or optimized through specially training a neural network (NN) during measurements dataset preprocessing [10]. Another approach is to adopt the weighted least absolute values (WLAV)-based estimator, which inherently mitigates the influence of outliers, eliminating the need for the processing of outliers and the time-consuming repeated estimation [11][12].

In recent years, data-driven approaches, particularly end-to-end (E2E) learning, have the potential to serve as a holistic framework with super performance to handle topology identification, PSSE and outliers processing altogether, provided adequate representative data are available for training [13]. For the RSE problem in this work, the E2E learning is naturally credited by its robustness to Non-Gaussian noise and outliers, and the near-instantaneous output in the online application, i.e. a NN can be trained offline to directly map noisy measurements to state variables [14]. However, the classical E2E learning approaches could not handle the physical constraints involved in the RSE problem, since it was initially developed for non-constrained problems [15]. Consequently, the resulted estimation may achieve high performance regression but are not guaranteed to be physical consistent [16].

To bridge this gap, one possible solution is to embed physical constraints into the E2E learning framework. A typical implementation involves designing a physics-informed neural network (PINN) by encoding physical constraints into a complicated and hybrid loss function [17] [18] [19]. As such, the PINN is just expected to generate solutions that are not only accurate but also physically consistent. In principle, the PINN approach may not generate the genuine optimal solution, since the Karush-Kuhn-Tucker (KKT) optimality conditions are not explicitly fulfilled and therefore constraint alignment cannot always be guaranteed [20].

Alternatively, embedding an independent differentiable optimization layer constructed from the constrained optimization problem itself into the NN structure has become a promising

This work has been submitted to the IEEE for possible publication. Copyright may be transferred without notice, after which this version may no longer be accessible.

solution [21]. Once trained properly, the outputs of such NN can largely ensure rigid alignment with physical constraints during online application, since the derivatives of the loss function with respect to problem parameters for backward propagation during training is derived from the KKT conditions [22]. Compared to the PINN, where the physical constraints are exogenously added into the loss function only, such a novel framework can thus significantly strengthen the constraint alignments in offering the optimal solutions of constrained optimization problems. This novel framework has been applied to AC optimal power flow [23][24] and voltage regulation [25], but has never been used in PSSE by far.

In this work, a novel E2E learning framework embedded with the differentiable optimization layer dedicated for RSE is proposed for the first time. Trained under a hybrid loss function gauging SE performance and physical consistency, the proposed framework is capable of estimating system states with significantly lowered residuals. Also, to render NN the active identification capability for more robustness against outliers, the measurement weights are treated as learnable parameters, which still remains notably underrepresented in existing literature.

A primary obstacle of implementing the aforementioned framework is the non-convexity of AC power flow equations as the constraints of the RSE problem [26]. Therefore, convex relaxation becomes necessary to derive the KKT conditions of the global optimal solution and then calculate the derivatives. Some relaxation techniques introduce auxiliary variables to linearize the power flow equations and impose second-order conic constraints on these variables, reformulating the problem as a second-order cone programming (SOCP) [27] [28]. However, a significant drawback is that the exactness can only be guaranteed for power grids with radial topology. The semidefinite relaxation is thus proposed for grids with either radial or meshed topologies [29], where the introduced auxiliary variables should satisfy a semidefinite constraint and a non-convex rank-one constraint. This relaxation is usually exact, especially when the rank-one solution can be obtained [30]. While methods such as rank reduction and convex iteration have been employed to tackle with the non-convexity of rank-one constraint [31], computational burdens arising from the semidefinite constraint exist. Correspondingly, gradient-based acceleration strategies [32] and conic relaxation [33] have been proposed to boost the tractability of relaxed problem. The semidefinite relaxation with a regularization term added into the RSE objective is utilized in our proposed E2E learning framework. The regularization term is designed to implicitly guide towards the rank-one solution. When applying for the RSE problem in this work, the relaxation exactness can be guaranteed given adequate observability under normal operation conditions, as detailed later.

The major contributions are summarized as follows. Firstly, a novel E2E learning framework is proposed for RSE. To the authors' best knowledge, this work is the first to both formulate the RSE problem as an independent differentiable layer within a NN and treat measurement weights as learnable parameters, enabling the NN to actively filter outliers towards higher estimation robustness in a holistic manner. Unlike PINN that

exogenously incorporating constraints violation as soft penalties, the proposed framework significantly improves overall estimation performances, as demonstrated through extensive simulations. Although the customized hybrid loss function weighing estimation accuracy and physical consistency is similar to that of PINN, a key advantage of the proposed framework lies in the rigorous KKT conditions embedding during backward propagation, achieving guaranteed physical consistency in estimated states. To realize this, differentiation of the relaxed RSE problem is specially carried out, where homogenization and implicit function theorem are utilized.

The proposed E2E learning framework is introduced in Section II. The RSE problem and the convex relaxation process are modeled in Section III. The loss function design, RSE problem differentiation and model training process are presented in Section IV. Section V analyzes the simulation results, and Section VI draws the conclusion.

II. FRAMEWORK OVERVIEW

Figure 1 demonstrates the proposed E2E learning framework for power system RSE problem. The input context of the NN includes noisy measurement data and the initial value of learnable weights of measurements. After offline training, the E2E learning framework can directly output the estimated states given real-time measurements in online implementation.

The NN in the proposed E2E framework is constructed by a differentiable optimization layer, named as 'Opt - Layer', and a set of post-processing layers. The Opt - Layer is rigorously and inherently embedded with physical constraints in the RSE problem, and the post-processing layers are responsible for solution recovery, namely mapping the resulting solutions of relaxed RSE problem into the space of decision variables of the original problem. The post-processing layers could be e.g. standard dense layers.

To realize strict physical constraints embedding in backward propagation, convex relaxation of the original RSE problem is necessary to obtain the KKT conditions of the global optimum. The mathematic details will be introduced in Section III. Specifically, the RSE problem is firstly relaxed into a semidefinite programming (SDP) by introducing auxiliary decision variables, and the corresponding semidefinite and rank-one constraints. Also, a regularization term is integrated into the objective to replace the non-convex rank-one constraint, which implicitly guides towards the rank-one solution. Then, the semidefinite constraint is further relaxed into a second-order conic constraint to reduce computational complexity. The SDP-based RSE problem is thus reformulated as a SOCP, which can be readily solved by commercial solvers. Then, through differentiating the SOCP-based RSE problem, rigorous KKT conditions embedding during backward propagation is achieved.

During the forward propagation, the NN takes the noisy measurements data and learnable measurement weights as input context. Then, the Opt - Layer would solve the relaxed RSE problems for all the samples in the training dataset, then output the estimated state variables after post-processing mapping. Noted that, problem sparsification is also necessary

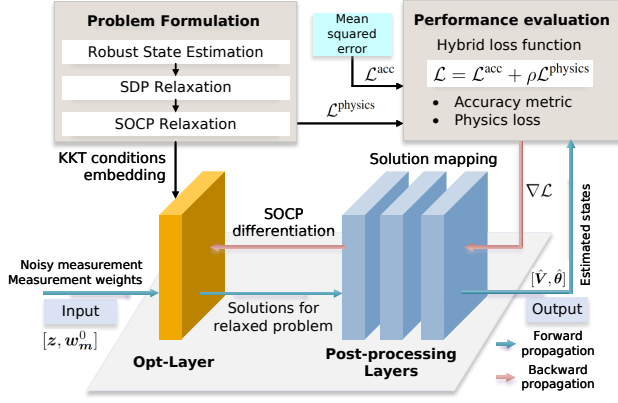


Fig. 1. The Proposed End-to-end Learning Framework for Power System Robust State Estimation.

in practical implementation to accelerate the training. To effectively guarantee the regression accuracy and physical consistency of the NN, a hybrid loss function \mathcal{L} weighing accuracy metric and physical loss is specially introduced, where the latter is derived from the objective of RSE problem, as modeled in Section IV.

During the backward propagation, the derivatives of the hybrid loss function $\nabla \mathcal{L}$ with respect to the learnable parameters of the NN are calculated. Specifically, the derivatives of optimal solutions of the relaxed problem with respect to the problem parameters are calculated by homogenizing the KKT conditions and utilizing implicit function theorem, which will be illustrated in Section IV-B. The NN is then trained offline via an algorithm such as stochastic gradient descent. Upon the completion of training, the NN learns a direct mapping from noisy measurements to the estimated nodal voltage magnitudes and phase angles, facilitating real-time applications.

III. PROBLEM FORMULATION

Given a fixed topology, the grid parameters could be defined as follows. Let $g_s + jb_s$ denote the series branch admittance between bus i and j ; b_c represents the line charging susceptance; k_t is the turns ratio of transformer; $g_{ij} = g_s/k_t$ and $b_{ij} = b_s/k_t$ are respectively the mutual conductance and susceptance between bus i and j ; $g_{si} = (1 - k_t)g_s/k_t^2$ and $b_{si} = (1 - k_t)b_s/k_t^2 + b_c/2$ are respectively the shunt conductance and susceptance at bus i to ground. Then, for simplicity, let $G_{ij} = -g_{ij}$, $B_{ij} = -b_{ij}$, $\hat{g}_{ij} = g_{si} + g_{ij}$ and $\hat{b}_{ij} = b_{si} + b_{ij}$. Also, let \mathcal{N} and \mathcal{N}_i respectively denote the set of all buses and the adjacent buses of bus i .

A. Classical Robust State Estimation Problem

Classical WLS-based PSSE provides unbiased estimates when the residuals follows a zero-mean Gaussian distribution [1]. In practical implementations, there might exist outliers in measurements, making the overall distribution of residuals distort from zero-mean Gaussian distribution. Also, the WLS-based estimator is highly sensitive to the outliers as the quadratic function of residuals. In contrast, the WLAV-based estimator, intrinsically a L1-norm minimization of residuals,

exhibits higher robustness against outliers. Accordingly, given a measurements dataset \mathcal{M} , a WLAV-based RSE model is formulated as follows [27]:

$$(P1) \quad \min_{V_i, \theta_i} \sum_{m \in \mathcal{M}} |\epsilon_m| / \sigma_m \quad (1)$$

subject to

$$z_{V_i} = V_i + \epsilon_{V_i} \quad (2)$$

$$z_{P_{ij}} = V_i^2 \hat{g}_{ij} - V_i V_j g_{ij} \cos \theta_{ij} - V_i V_j b_{ij} \sin \theta_{ij} + \epsilon_{P_{ij}} \quad (3)$$

$$z_{Q_{ij}} = -V_i^2 \hat{b}_{ij} + V_i V_j b_{ij} \cos \theta_{ij} - V_i V_j g_{ij} \sin \theta_{ij} + \epsilon_{Q_{ij}} \quad (4)$$

$$z_{P_i} = V_i \sum_{j \in \mathcal{N}_i} V_j (G_{ij} \cos \theta_{ij} + B_{ij} \sin \theta_{ij}) + \epsilon_{P_i} \quad (5)$$

$$z_{Q_i} = V_i \sum_{j \in \mathcal{N}_i} V_j (G_{ij} \sin \theta_{ij} - B_{ij} \cos \theta_{ij}) + \epsilon_{Q_i} \quad (6)$$

where z and ϵ are respectively the measurements data and residual. σ_m is the weight of the m -th measurements data, where $m \in \{V_i, P_{ij}, Q_{ij}, P_i, Q_i\}$. V_i is the voltage magnitude of bus i . θ_{ij} is the phase angle difference between bus i and j . P_{ij} and Q_{ij} are respectively the active and reactive line power flow between bus i and j . P_i and Q_i are respectively the total active and reactive power injection of bus i .

Remark: The WLAV-based estimator yields unbiased estimates when the residuals follow a Laplace distribution [34], which has fatter tails than standard Gaussian distribution, providing inherent robustness against almost inevitable outliers. Although the practical statistical distribution of residuals may not strictly follow a Laplace distribution, the WLAV-based estimator still demonstrates more robust performance than the WLS-based estimator, rendering its suitability for applications.

B. Convex Relaxation

Although (P1) effectively suppresses the impact of outliers, it introduces undesired non-convexity because of the quadratic voltage magnitudes and products of voltage magnitudes with trigonometric functions of phase angles in the constraints (3)-(6). To alleviate the computational burden and pave the way for rigorous physical constraints embedding, convex relaxation for (P1) is necessary.

The relaxation is achieved by introducing an auxiliary complex matrix $\mathbf{X} = \mathbf{V}\mathbf{V}^* \in \mathbb{C}^{|\mathcal{N}| \times |\mathcal{N}|}$ to linearize (3)-(6), where $\mathbf{V} \in \mathbb{C}^{|\mathcal{N}|}$ is the complex voltage vector and $\mathbf{V}_i = V_i \angle \theta_i$. \mathbf{V}^* is the conjugate of \mathbf{V} . The diagonal elements of \mathbf{X} are given by $X_{ii} = V_i^2$, while the off-diagonal elements are $X_{ij} = V_i V_j (\cos \theta_{ij} + j \sin \theta_{ij})$.

Theorem 1: The equality $\mathbf{X} = \mathbf{V}\mathbf{V}^*$ holds if and only if the following two conditions are met: (1) $\mathbf{X} \succeq \mathbf{0}$; and (2) $\text{rank}(\mathbf{X}) = 1$ [30].

Condition (1) can be readily enforced by adding a positive semidefinite constraint. Nevertheless, Condition (2), $\text{rank}(\mathbf{X}) = 1$, is still non-convex and poses computational challenge. Therefore, a regularization term is introduced into the objective to guide towards the rank-one solution. The conditions for the exactness of this relaxation are discussed in Appendix A.

Corollary 1: The introduced regularization term exactly calculates the total active power loss of the power system. A proof is provided in Appendix B.

The resulting problem (P2) is formulated as follows:

$$(P2) \min_{\mathbf{X}} \rho_r \sum_{m \in \mathcal{M}} |\epsilon_m|/\sigma_m + \text{Re}(\sum_{i \in \mathcal{N}} \sum_{j \in \mathcal{N}} Y_{ij}^* X_{ij}) \quad (7)$$

subject to

$$z_{V_i^2} = X_{ii} + \epsilon_{V_i^2} \quad (8)$$

$$z_{P_{ij}} = X_{ii} \hat{g}_{ij} - g_{ij} \text{Re}(X_{ij}) - b_{ij} \text{Im}(X_{ij}) + \epsilon_{P_{ij}} \quad (9)$$

$$z_{Q_{ij}} = -X_{ii} \hat{b}_{ij} + b_{ij} \text{Re}(X_{ij}) - g_{ij} \text{Im}(X_{ij}) + \epsilon_{Q_{ij}} \quad (10)$$

$$z_{P_i} = \sum_{j \in \mathcal{N}_i} (G_{ij} \text{Re}(X_{ij}) + B_{ij} \text{Im}(X_{ij})) + \epsilon_{P_i} \quad (11)$$

$$z_{Q_i} = \sum_{j \in \mathcal{N}_i} (G_{ij} \text{Im}(X_{ij}) - B_{ij} \text{Re}(X_{ij})) + \epsilon_{Q_i} \quad (12)$$

$$\mathbf{X} \succeq \mathbf{0} \quad (13)$$

where $\rho_r > 0$ is the weighting coefficient. Y_{ij} is the off-diagonal element in the nodal admittance matrix. $\text{Re}(\cdot)$ and $\text{Im}(\cdot)$ are respectively the real and imaginary part of a complex variable. The second term in the objective function is the regularization term, which is actually a linear function with respect to decision variables, namely $G_{ij} \text{Re}(X_{ij}) + B_{ij} \text{Im}(X_{ij})$. Constraint (13) stands for the Condition (1).

The decision variables of (P2) now are composed by X_{ii} , $\text{Re}(X_{ij})$ and $\text{Im}(X_{ij})$. Also, (3)-(6) are all linearized in (9)-(12). (P2) is therefore convexified into a SDP problem.

C. Second-order Conic Relaxation

To further alleviate the computational expense of (P2), the positive semidefinite constraint (13) can be relaxed into a set of more tractable second-order cone constraints.

Theorem 2: If a matrix is positive semidefinite, all of its principal submatrices must also be positive semidefinite.

Given the above theorem, (P2) can be exactly reformulated as the following SOCP problem (P3):

$$(P3) \min_{\mathbf{X}} \rho_r \sum_{m \in \mathcal{M}} |\epsilon_m|/\sigma_m + \text{Re}(\sum_{i \in \mathcal{N}} \sum_{j \in \mathcal{N}} Y_{ij}^* X_{ij}) \quad (14)$$

subject to (8)-(12),

$$\|2\text{Re}(X_{ij}), 2\text{Im}(X_{ij}), X_{ii} - X_{jj}\|_2 \leq X_{ii} + X_{jj} \quad (15)$$

D. Solution Recovery

After solving the relaxed RSE problem (P3), it is necessary to recover the original estimated states \mathbf{V} from the relaxed solutions \mathbf{X} . According to Theorem 1, the rank-one solution, denoted as \mathbf{X}° , can be decomposed into the outer product of \mathbf{V} and its conjugate \mathbf{V}^* .

Then, by multiplying \mathbf{V} , we have:

$$\mathbf{X}^\circ \mathbf{V} = \mathbf{V}(\mathbf{V}^* \mathbf{V}) = \mathbf{V} \|\mathbf{V}\|^2 \quad (16)$$

This indicates that \mathbf{V} is an eigenvector of \mathbf{X}° , with the unique non-zero eigenvalue of $\|\mathbf{V}\|^2$. Since \mathbf{X}° is a Hermitian positive semidefinite matrix, an eigenvalue decomposition can be performed as:

$$\mathbf{X}^\circ = \mathbf{U}_e \mathbf{\Lambda} \mathbf{U}_e^* \quad (17)$$

where the eigenvalue matrix $\mathbf{\Lambda}$ contains only one significant non-zero eigenvalue $\lambda = \|\mathbf{V}\|^2$, with the corresponding

eigenvector $\mathbf{u} = \mathbf{V}/\|\mathbf{V}\|$. All the other eigenvalues will be theoretically zero.

Then, the complex voltage vector \mathbf{V} could be recovered by:

$$\mathbf{V} = \|\mathbf{V}\| \mathbf{u} = \sqrt{\lambda} \mathbf{u} \quad (18)$$

Finally, the estimated voltage magnitude \hat{V} and phase angle $\hat{\theta}$ could be exactly extracted based on \mathbf{V} .

IV. END-TO-END LEARNING FOR POWER SYSTEM ROBUST STATE ESTIMATION

A. Loss Function Design

To obtain accurate and physical consistent estimated states through the proposed E2E learning framework, a hybrid loss function \mathcal{L} is defined as follows:

$$\mathcal{L} = \mathcal{L}^{\text{acc}} + \rho \mathcal{L}^{\text{physics}} \quad (19)$$

$$\mathcal{L}^{\text{physics}} = \sum_{m \in \mathcal{M}} w_m |\epsilon_m| + \text{Re}(\sum_{i \in \mathcal{N}} \sum_{j \in \mathcal{N}} Y_{ij}^* X_{ij}) \quad (20)$$

where \mathcal{L}^{acc} is a differentiable accuracy metric measuring the distance between actual true states and estimated states, such as mean squared error (MSE). $\mathcal{L}^{\text{physics}}$ represents the physical inconsistency loss, composed of the WLAV of residuals and the regularization term. w_m is the learnable weight of the m -th measurement data. ρ is a hyperparameter indicating the importance of physical loss.

Noted that, the non-smoothness of $|\epsilon_m|$ in $\mathcal{L}^{\text{physics}}$ is an obstacle of differentiation. Therefore, a surrogate loss term called as Huber loss is introduced as follows to guarantee the smoothness [35]. Specifically, in the neighborhood of origin $\epsilon_m \in [-\delta, \delta]$, the Huber loss is defined as the quadratic function of residuals, otherwise the loss is linear.

Moreover, it is crucial to prevent the NN from cheating by assigning negative values to the learnable weights w_m to minimize the loss. To enforce the positivity of w_m , a mapping is applied in (22). Softplus function is specifically selected for its advantageous properties of being smooth and continuously differentiable. Besides, to ensure strict positivity and improve numerical stability, a small positive constant ϵ_p is added.

$$\mathcal{L}^{\text{huber}} = \begin{cases} \sum_{m \in \mathcal{M}} \hat{w}_m (\epsilon_m)^2 / 2, & \text{for } |\epsilon_m| \leq \delta, \\ \sum_{m \in \mathcal{M}} \hat{w}_m \delta (|\epsilon_m| - \delta / 2), & \text{otherwise.} \end{cases} \quad (21)$$

$$\hat{w}_m = \ln(1 + e^{w_m}) + \epsilon_p, \quad \forall m \in \mathcal{M} \quad (22)$$

When $\delta \rightarrow 0$, Huber loss function degenerates into the original WLAV-based loss, ensuring its less sensitivity to outliers in noisy measurement data than the quadratic WLS-based loss. To conclude, the surrogate physical loss and hybrid loss could be defined as:

$$\hat{\mathcal{L}}^{\text{physics}} = \mathcal{L}^{\text{huber}} + \mathcal{L}^{\text{reg}} \quad (23)$$

$$\hat{\mathcal{L}} = \mathcal{L}^{\text{acc}} + \rho \hat{\mathcal{L}}^{\text{physics}} \quad (24)$$

where \mathcal{L}^{reg} denotes the value of regularization term, which also calculates the total active power loss for simplicity.

Remark: Compared to linearizing the L1-norm term in (20), using Huber loss function as surrogate in training would not bring about extra decision variables and constraints, avoiding

extra computational burden during training. Also, Huber loss function achieves near-exact approximation when δ is sufficiently close to 0.

B. Differentiating the RSE Problem

This subsection derives the derivative of the optimal solution \mathbf{X}° of relaxed RSE problem (P3) with respect to the problem parameters, including grid parameters and input measurements \mathbf{z} , for backward propagation calculation.

1) *Problem Reformulation*: Firstly, the primal and dual forms of SOCP-based RSE problem (P3) could be rewritten in compact form as follows for simplicity:

$$\begin{aligned} \text{(Primal)} \quad & \min \mathbf{c}^\top \mathbf{x} & \text{(Dual)} \quad & \min \mathbf{b}^\top \mathbf{y} \\ \text{s.t.} \quad & \mathbf{A}\mathbf{x} + \mathbf{s} = \mathbf{b} & \text{s.t.} \quad & \mathbf{A}^\top \mathbf{y} + \mathbf{c} = \mathbf{0} \\ & \mathbf{s} \in \mathcal{K} & & \mathbf{y} \in \mathcal{K}^* \end{aligned} \quad (25)$$

where $\mathbf{x} \in \mathbb{R}^p$ collects all the primal decision variables, namely all the $X_{ii}, \text{Re}(X_{ij}), \text{Im}(X_{ij})$. $\mathbf{y} \in \mathbb{R}^d$ integrates the dual variables. \mathbf{s} is the primal slack variable. $\mathcal{K} \subseteq \mathbb{R}^d$ is a nonempty, closed and convex cone, whose dual cone is denoted by $\mathcal{K}^* \subseteq \mathbb{R}^d$. The optimal solution of the above problem is bound to satisfy the following KKT conditions:

$$\begin{cases} \mathbf{A}\mathbf{x} + \mathbf{s} = \mathbf{b}, \\ \mathbf{A}^\top \mathbf{y} + \mathbf{c} = \mathbf{0}, \\ \mathbf{s} \in \mathcal{K}, \quad \mathbf{y} \in \mathcal{K}^*, \\ \mathbf{s}^\top \mathbf{y} = \mathbf{0}. \end{cases} \quad (26)$$

2) *Differentiation Decomposition*: In this subsection, our objective is to derive the analytical derivative of the mapping from problem parameters $(\mathbf{A}, \mathbf{b}, \mathbf{c})$ to the optimal solution $(\mathbf{x}^*, \mathbf{y}^*, \mathbf{s}^*)$ for backward propagation, denoted as $\Pi : \mathbb{R}^{d \times p} \times \mathbb{R}^d \times \mathbb{R}^p \rightarrow \mathbb{R}^{p+2d}$.

The mapping Π could be decomposed into three sub-mappings $\phi \circ g \circ \Omega$, where \circ is the function composition operator. Specifically, let $D_1 = p+d+1$ and $D_2 = p+2d+2$, $\Omega : \mathbb{R}^{d \times p} \times \mathbb{R}^d \times \mathbb{R}^p \rightarrow \mathbb{R}^{D_1 \times D_2}$ maps the problem parameters to an auxiliary matrix Ω . $g : \mathbb{R}^{D_1 \times D_2} \rightarrow \mathbb{R}^{D_2}$ is the mapping from Ω to the solution of the homogeneous self-dual system (HSDS), which will be introduced in the next subsection. $\phi : \mathbb{R}^{D_2} \rightarrow \mathbb{R}^{p+2d}$ recovers the optimal solution of (25). Then, the derivative of forward propagation ∇_{Π} can be calculated as follows:

$$\nabla_{\Pi}(\mathbf{A}, \mathbf{b}, \mathbf{c}) = \nabla_{\Omega}(\mathbf{A}, \mathbf{b}, \mathbf{c}) \nabla_g(\Omega(\mathbf{A}, \mathbf{b}, \mathbf{c})) \nabla_{\phi}(g(\Omega)) \quad (27)$$

For backward propagation, the resulting adjoint derivative ∇_{Π}^\top could be calculated as follows:

$$\left(\frac{\partial \mathcal{L}}{\partial \mathbf{A}}, \frac{\partial \mathcal{L}}{\partial \mathbf{b}}, \frac{\partial \mathcal{L}}{\partial \mathbf{c}} \right) = \nabla_{\Pi}^\top(\mathbf{A}, \mathbf{b}, \mathbf{c}) \left(\frac{\partial \mathcal{L}}{\partial \mathbf{x}}, \frac{\partial \mathcal{L}}{\partial \mathbf{y}}, \frac{\partial \mathcal{L}}{\partial \mathbf{s}} \right) \quad (28)$$

$$\nabla_{\Pi}^\top(\mathbf{A}, \mathbf{b}, \mathbf{c}) = \nabla_{\phi}^\top(g(\Omega)) \nabla_g^\top(\Omega(\mathbf{A}, \mathbf{b}, \mathbf{c})) \nabla_{\Omega}^\top(\mathbf{A}, \mathbf{b}, \mathbf{c}) \quad (29)$$

3) *Pre-processing Problem Parameters*: To calculate the analytical expressions for each component in (27), the auxiliary matrix Ω is firstly constructed to pre-process the problem

parameters $(\mathbf{A}, \mathbf{b}, \mathbf{c})$ as follows:

$$\Omega = \begin{bmatrix} \mathbf{0} & \mathbf{A}^\top & \mathbf{0} & \mathbf{c} & \mathbf{0} \\ -\mathbf{A} & \mathbf{0} & \mathbf{I} & \mathbf{b} & \mathbf{0} \\ -\mathbf{c}^\top & -\mathbf{b}^\top & \mathbf{0} & \mathbf{0} & \mathbf{I} \end{bmatrix}. \quad (30)$$

Correspondingly, the derivative of the mapping from $(\mathbf{A}, \mathbf{b}, \mathbf{c})$ to Ω can be calculated as follows:

$$\nabla_{\Omega}(\mathbf{A}, \mathbf{b}, \mathbf{c}) = \begin{bmatrix} \mathbf{0} & \frac{\partial \mathcal{L}}{\partial \mathbf{A}^\top} & \mathbf{0} & \frac{\partial \mathcal{L}}{\partial \mathbf{c}} & \mathbf{0} \\ -\frac{\partial \mathcal{L}}{\partial \mathbf{A}} & \mathbf{0} & \mathbf{0} & \frac{\partial \mathcal{L}}{\partial \mathbf{b}} & \mathbf{0} \\ -\frac{\partial \mathcal{L}}{\partial \mathbf{c}^\top} & -\frac{\partial \mathcal{L}}{\partial \mathbf{b}^\top} & \mathbf{0} & \mathbf{0} & \mathbf{0} \end{bmatrix}. \quad (31)$$

4) *Homogeneous Self-Dual Embedding*: Then, the mapping g embeds the original problem (25) into a higher-dimensional HSDS, transforming the task of optimizing (25) into finding a non-trivial solution to a set of equations, thereby significantly reducing the computational complexity. In other words, the KKT conditions are homogenized into the following system:

$$\begin{cases} \mathbf{A}\mathbf{x} + \mathbf{s} - \mathbf{b}\tau = \mathbf{0}, & \text{(Primal feasibility residual),} \\ \mathbf{A}^\top \mathbf{y} + \mathbf{c}\tau = \mathbf{0}, & \text{(Dual feasibility residual),} \\ -\mathbf{b}^\top \mathbf{y} - \mathbf{c}^\top \mathbf{x} - \kappa = 0, & \text{(Duality gap residual),} \\ \mathbf{s}^\top \mathbf{y} + \tau\kappa = 0, & \text{(Complementary slackness),} \\ \mathbf{s} \in \mathcal{K}, \quad \mathbf{y} \in \mathcal{K}^*, \tau \geq 0, \kappa \geq 0. \end{cases} \quad (32)$$

where the decision variables could be collected as $\mathbf{h} = (\mathbf{x}, \mathbf{y}, \mathbf{s}, \tau, \kappa) \in \mathbb{R}^{D_2}$. τ is a scaling factor. κ is an optimality indicator.

Subsequently, (32) can be compactly rewritten as a linear system given the auxiliary matrix Ω :

$$F(\mathbf{h}, \Omega) = \Omega \mathbf{h} + \mathbf{t} = \mathbf{0} \quad (33)$$

where $\mathbf{t} \in \mathbb{R}^{D_1}$ is the slack variable.

Since the non-trivial solution $\mathbf{h}^* \neq \mathbf{0}$ of (33) is actually an implicit function of Ω , written as $\mathbf{h}^* = g(\Omega)$. The derivative of \mathbf{h}^* with respect to Ω can be calculated as follows without acquiring specific mathematical form of $g(\cdot)$ by utilizing the implicit function theorem [36]:

$$\nabla_g(\Omega) = -[(\partial F / \partial \mathbf{h})^{-1}] (\partial F / \partial \Omega). \quad (34)$$

5) *Solution Mapping*: The HSDS in (32) is always feasible, as it is guaranteed to have a trivial solution, i.e., $\mathbf{0}$. If we could find a non-trivial solution satisfying $\tau > 0$, all the decision variables \mathbf{h} can be scaled by dividing by τ . Due to the complementary slackness conditions, there is $\kappa = 0$. The resulting optimal solution $(\mathbf{x}^\circ / \tau, \mathbf{y}^\circ / \tau, \mathbf{s}^\circ / \tau)$ then precisely satisfies the KKT conditions in (26), demonstrating that this solution is exactly the optimal solution to the problem (25). Therefore, given the optimal solution of HSDS \mathbf{h}^* , we have:

$$(\mathbf{x}^*, \mathbf{y}^*, \mathbf{s}^*) = \left(\frac{\mathbf{x}^\circ}{\tau}, \frac{\mathbf{y}^\circ}{\tau}, \frac{\mathbf{s}^\circ}{\tau} \right) = \phi(\mathbf{x}^\circ, \mathbf{y}^\circ, \mathbf{s}^\circ, \tau, \kappa). \quad (35)$$

$$\nabla_{\phi}(\mathbf{h}) = \begin{bmatrix} \mathbf{I}_p / \tau & \mathbf{0} & \mathbf{0} & -\mathbf{x} / \tau^2 & \mathbf{0} \\ \mathbf{0} & \mathbf{I}_d / \tau & \mathbf{0} & -\mathbf{y} / \tau^2 & \mathbf{0} \\ \mathbf{0} & \mathbf{0} & \mathbf{I}_d / \tau & -\mathbf{s} / \tau^2 & \mathbf{0} \end{bmatrix} \quad (36)$$

where $\mathbf{I}_p \in \mathbb{R}^p$ and $\mathbf{I}_d \in \mathbb{R}^d$ are identity matrices.

C. E2E Decision-making Model Training Process

Building upon the NN architecture established in Section II and the relaxed SOCP-based RSE problem (P3) derived in Section III, Algorithm 1 details the proposed E2E learning algorithm for power system RSE. The procedure commences with the generation of a dataset. The input features consist of measurements \mathbf{z} , which can be sourced from actual SCADA devices or generated through numerical simulations, while the output labels are the corresponding system states \mathbf{V} . After defining necessary hyperparameters and partitioning the dataset \mathcal{D} into training set $\mathcal{D}_{\text{train}}$ and testing set $\mathcal{D}_{\text{test}}$, the relaxed problem (P3) is parametrically modeled to construct the differentiable Opt – Layer with embedded physical constraints [26].

During the training stage, the NN processes batches from the $\mathcal{D}_{\text{train}}$. The set of learnable parameters for the entire NN $\boldsymbol{\mu}$ includes the measurement weights \mathbf{w}_m within the Opt – Layer, as well as the weights and biases of the post-processing layers. In the forward propagation, as described in Section II, the Opt – Layer first solves the relaxed problems (P3) in the batch, and the post-processing layers then map these solutions back to the original variables space. In the backward propagation, derivatives are computed via the chain rule. Specifically, the derivatives of the loss function $\hat{\mathcal{L}}$ with respect to the parameters of post-processing layers are calculated first, followed by the derivatives with respect to the learnable measurement weights \mathbf{w}_m using the method detailed in Section IV-B. Subsequently, all learnable parameters $\boldsymbol{\mu}$ across the NN are updated. Moreover, to ensure efficient convergence and reduce sensitivity to hyperparameter tuning, the adaptive moment estimation (Adam) optimizer is employed. Furthermore, weight decay technique is incorporated to mitigate the risk of overfitting.

Once training is complete, the resulting NN provides a direct mapping from raw measurement inputs to the estimated system states. This enables online deployment, a significant advantage over traditional optimization-based approaches, whose computational demands often limit their potential for real-time applications.

D. Sparsification

A critical consideration for practical implementation is the computational burden associated with the Opt – Layer, particularly for large-scale systems. Although the dimension of final estimated states is $2|\mathcal{N}|$, the decision variables of the relaxed problem (P3) include $\text{Re}(X_{ij}) \in \mathbb{R}^{|\mathcal{N}| \times |\mathcal{N}|}$ and $\text{Im}(X_{ij}) \in \mathbb{R}^{|\mathcal{N}| \times |\mathcal{N}|}$. This results in a stacked Opt – Layer output dimension of $|\mathcal{N}| + 2|\mathcal{N}|^2$, indicating an unacceptable computational cost during forward propagation.

The inherent sparsity of the nodal admittance matrix Y is utilized to address this challenge. In a power system, $Y_{ij} = 0$ signifies that no direct branch connects bus i and j . Consequently, the corresponding element X_{ij} is also zero. Therefore, in our work, only $\text{Re}(X_{ij})$ and $\text{Im}(X_{ij})$ are treated as active decision variables for the bus pairs (i, j) where $Y_{ij} \neq 0$. All the other elements of X_{ij} are fixed to zero. This

Algorithm 1 E2E Learning Algorithm for Power System Robust State Estimation

- 1: **Dataset preparation:** Prepare the full dataset $\mathcal{D} = \{\mathbf{z}, \mathbf{V}\}$, containing measurement data \mathbf{z} as input feature, states variables \mathbf{V} as output label. Hyperparameters (learning rate α , weight decay factor ζ , batch size B , training epoch E , physical loss weight factor ρ).
 - 2: **Dataset separation:** Dataset \mathcal{D} is separated into training dataset $\mathcal{D}_{\text{train}}$ and testing dataset $\mathcal{D}_{\text{test}}$;
 - 3: **Layer construction:** Formulate parametrized relaxed RSE problem based on (P3) and construct the Opt – Layer;
 - 4: **Offline training:**
 - 5: Input training dataset $\mathcal{D}_{\text{train}}$, initial measurement weights \mathbf{w}_m^0 ;
 - 6: **for** epoch = 1, ..., E **do**
 - 7: **Forward propagation:**
 - 8: *Decision-making:* solve the parametrized relaxed problems in each batch via Opt – Layer;
 - 9: *Post-processing:* map the solutions for relaxed problems for recovery, obtaining estimated $\hat{\mathbf{V}}$;
 - 10: **Backward propagation:**
 - 11: Calculate the derivative of surrogate loss function with respect to all the learnable parameters $\boldsymbol{\mu}$ as $\nabla_{\boldsymbol{\mu}} \hat{\mathcal{L}}$;
 - 12: **Parameters updating:**
 - 13: Update the learnable parameters of NN.
 - 14: **end for**
 - 15: Obtain the trained E2E learning model.
 - 16: **Online application:**
 - 17: *Decision-making:* Input testing dataset $\mathcal{D}_{\text{test}}$, output estimated state variables $\hat{\mathbf{V}}$.
 - 18: *Performance evaluation:* Calculate accuracy loss \mathcal{L}^{acc} and physical loss $\mathcal{L}^{\text{physics}}$.
-

strategy drastically reduces the numbers of decision variables and constraints, realizing significantly accelerated training.

V. CASES STUDIES

A. Parameters setup

To validate the performance of the proposed E2E learning framework, extensive simulations are conducted on six testing power systems with both radial and meshed topologies. The grid parameters are extracted from the Matpower case files. By assuming the measurement completeness, the measurement set in this work includes all nodal voltage magnitudes, branch power flows, and nodal power injections.

The dataset for each system is constructed as follows. First, true system states are obtained by running probabilistic power flow calculations using the given parameters in Matpower cases files. Measurements are then simulated by adding zero-mean Gaussian noise, with a standard deviation of $\sigma_m = 0.001$ p.u., to these ground-truth values. Outliers are simulated by amplifying the σ_m by a scaling factor of k under a certain penetration rate η . For simplicity, the coefficient ρ_r in the objectives of (P2) and (P3) is set as 1. δ and ϵ_p are together set as $1e-5$ to formulate the Huber loss function.

The hyperparameters configured for the E2E learning framework are set as follows: learning rate $\alpha = 1e-3$, weight

TABLE I
SETTINGS OF DIFFERENT E2E LEARNING MODELS

| Model | NN structure | Loss function |
|-------|------------------|-----------------------|
| #1 | Opt-Layer + FCNN | Surrogate hybrid loss |
| #2 | FCNN | Surrogate hybrid loss |
| #3 | CNN | Surrogate hybrid loss |
| #4 | FCNN | MSE |
| #5 | CNN | MSE |

decay factor $\zeta = 5e - 4$, batch size $B = 32$, training epoch $E = 300$. In particular, a sensitivity analysis on the selection of the physical loss weight ρ within the hybrid loss function is presented in Section V-D. The exponential decay rates of Adam, denoted by β_1 and β_2 , are set as 0.9 and 0.999 by default. For each testing system, 500 samples are partitioned into a training set $\mathcal{D}_{\text{train}}$ and a testing set $\mathcal{D}_{\text{test}}$ at an 8:2 ratio. All simulations are implemented by Matlab 2024a and Python 3.10 with PyTorch and CVXPY packages on a personal computer and optimization problems are solved by Gurobi. The hardware environment is Intel i7-14700F CPU and NVIDIA GeForce RTX 4060Ti GPU.

B. Robustness Comparison Using Different Estimators

To demonstrate the robustness of the WLAV estimator against varying levels of outlier penetration, simulations on IEEE-9 bus testing system are conducted. Five sets of parameters are set as follows. Case #1: $\eta = 0\%$, without outliers. Case #2: $\eta = 15\%$, $k = 10$. Case #3: $\eta = 15\%$, $k = 50$. Case #4: $\eta = 30\%$, $k = 10$. Case #5: $\eta = 30\%$, $k = 50$. Under each setting, 200 scenarios are generated.

Fig. 2 compares the root mean square error (RMSE) of estimated voltage magnitude and phase angle using WLAV-based and WLS-based estimators. In Fig. 2 (a), the medians of voltage magnitude RMSE using WLAV-based estimator are between [0.022, 0.023] p.u., while the results of WLS-based estimator are within the range of [0.0254, 0.0258] p.u.. Similarly, the medians of angle RMSE using WLAV-based and WLS-based estimators fall into the range of [0.063, 0.064] p.u. and [0.0794, 0.0796] p.u., respectively. Obviously, the errors obtained from WLAV-based estimator are all statistically significantly lower under different settings of outliers penetration. Also, as η and k increase, the distribution of errors become more dispersed, reflecting a higher proportion of large estimation errors. These results confirm that the WLS-based estimator is more sensitive to outliers due to the quadratic residual term in its objective, whereas the WLAV-based estimator demonstrates higher robustness.

C. Performances Comparison Using Different Learning Models

To validate the physical consistency of estimated states obtained by the proposed E2E learning framework, comparative experiments using five E2E learning models are carried out. The model settings are detailed in Tabel I. The proposed framework is denoted as Model #1, whose NN structure is the combination of a differentiable Opt – Layer and a set of

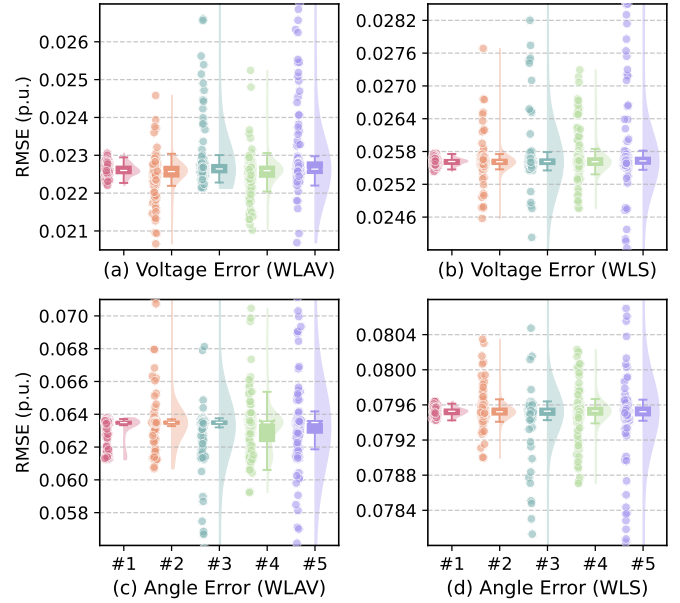


Fig. 2. Estimation Robustness Comparison on IEEE-9 Bus System.

fully connected post-processing layers, as described in Section II. The Opt – Layer is constructed from the relaxed RSE problem itself, ensuring strict optimality conditions embedding during back propagation. Model #1, #2 and #3 are trained using the surrogate hybrid loss function $\hat{\mathcal{L}}$, where the physical loss weight ρ is set to 1 for simplicity. The other learning models consist of standard fully connected neural network (FCNN) and convolution neural network (CNN) architectures. Noted that, Model #2 and #3 are actually PINNs. Also, to highlight the role of the hybrid loss function, experiments using a pure accuracy-oriented loss function (i.e., MSE) are also included for comparison in Model #4 and #5. The estimation results obtained from commercial solvers, e.g. Gurobi, serve as benchmarks for a more comprehensive comparison.

To demonstrate the generalizability of the proposed E2E learning framework, these models are all validated across six typical testing systems, encompassing both radial (IEEE-33 and IEEE-136) and meshed topologies (IEEE-9, IEEE-14, IEEE-39 and IEEE-57). As illustrated in Algorithm 1, the input context of the NN includes the measurements data and the initial value for the learnable measurement weights w_m^0 , which is set as 1 to ensure numerical stability.

Table II compares the performances of the five E2E learning models and Gurobi on four metrics: total surrogate hybrid loss $\hat{\mathcal{L}}$, MSE-based regression accuracy error \mathcal{L}^{acc} , surrogate estimation residuals $\mathcal{L}^{\text{huber}}$, and the regularization term standing for total active power losses \mathcal{L}^{reg} . The best results among learning models for each metric are highlighted in bold.

Collectively, the results demonstrate that Model #1 achieves the best physical consistency across all testing systems, proving the effectiveness of the proposed E2E learning framework with Opt – Layer in constrained optimization problems such as RSE. The estimation residuals are the lowest among all the E2E learning models, proving the effectiveness of strict fulfillment of constraints through KKT conditions embedding

TABLE II
ESTIMATION PERFORMANCES COMPARISON USING DIFFERENT E2E LEARNING MODELS.

| Model | IEEE-9 | | | | IEEE-14 | | | | IEEE-33 | | | |
|--------|---------------------|----------------------------|------------------------------|----------------------------|---------------------|----------------------------|------------------------------|----------------------------|---------------------|----------------------------|------------------------------|----------------------------|
| | $\hat{\mathcal{L}}$ | \mathcal{L}^{acc} | $\mathcal{L}^{\text{huber}}$ | \mathcal{L}^{reg} | $\hat{\mathcal{L}}$ | \mathcal{L}^{acc} | $\mathcal{L}^{\text{huber}}$ | \mathcal{L}^{reg} | $\hat{\mathcal{L}}$ | \mathcal{L}^{acc} | $\mathcal{L}^{\text{huber}}$ | \mathcal{L}^{reg} |
| #1 | 0.01158 | 0.00168 | 0.00966 | 0.00024 | 0.00640 | 0.00143 | 0.00437 | 0.00060 | 0.17559 | 0.04311 | 0.09483 | 0.03765 |
| #2 | 0.10219 | 0.00184 | 0.09884 | 0.00151 | 0.03592 | 0.00157 | 0.03229 | 0.00205 | 0.35506 | 0.10160 | 0.21113 | 0.04233 |
| #3 | 0.10211 | 0.00182 | 0.09891 | 0.00138 | 0.03633 | 0.00167 | 0.03221 | 0.00244 | 0.66137 | 0.42701 | 0.23166 | 0.00270 |
| #4 | 0.21328 | 0.00003 | 0.16752 | 0.04573 | 0.17979 | 0.00001 | 0.04969 | 0.13009 | 0.53845 | 0.00019 | 0.30459 | 0.23367 |
| #5 | 0.20096 | 0.00027 | 0.15770 | 0.04299 | 0.17222 | 0.00015 | 0.04804 | 0.12404 | 0.68120 | 4e-6 | 0.41556 | 0.26564 |
| Gurobi | 0.00943 | 0.00201 | 0.00738 | 0.00004 | 0.00501 | 0.00193 | 0.00305 | 0.00002 | 0.49034 | 0.44393 | 0.04638 | 0.00003 |

| Model | IEEE-39 | | | | IEEE-57 | | | | IEEE-136 | | | |
|--------|---------------------|----------------------------|------------------------------|----------------------------|---------------------|----------------------------|------------------------------|----------------------------|---------------------|----------------------------|------------------------------|----------------------------|
| | $\hat{\mathcal{L}}$ | \mathcal{L}^{acc} | $\mathcal{L}^{\text{huber}}$ | \mathcal{L}^{reg} | $\hat{\mathcal{L}}$ | \mathcal{L}^{acc} | $\mathcal{L}^{\text{huber}}$ | \mathcal{L}^{reg} | $\hat{\mathcal{L}}$ | \mathcal{L}^{acc} | $\mathcal{L}^{\text{huber}}$ | \mathcal{L}^{reg} |
| #1 | 0.18310 | 0.00316 | 0.16269 | 0.01725 | 0.00980 | 0.00148 | 0.00736 | 0.00096 | 0.48883 | 0.47248 | 0.01325 | 0.00310 |
| #2 | 0.80778 | 0.00343 | 0.75707 | 0.04729 | 0.04160 | 0.00193 | 0.03694 | 0.00273 | 0.57156 | 0.47395 | 0.08787 | 0.00974 |
| #3 | 0.83496 | 0.01347 | 0.78464 | 0.03685 | 0.04214 | 0.00225 | 0.03724 | 0.00265 | 0.62584 | 0.47157 | 0.08783 | 0.06644 |
| #4 | 1.44017 | 0.00049 | 0.96054 | 0.47915 | 0.32606 | 0.00001 | 0.04634 | 0.27971 | 1.75455 | 0.00064 | 0.83121 | 0.92269 |
| #5 | 1.30032 | 0.00020 | 0.88813 | 0.41198 | 0.33734 | 0.00005 | 0.04882 | 0.28847 | 1.05277 | 0.00017 | 0.53761 | 0.51499 |
| Gurobi | 0.11427 | 0.04753 | 0.06623 | 0.00051 | 0.05401 | 0.04913 | 0.00484 | 0.00004 | 0.53347 | 0.52489 | 0.00856 | 0.00002 |

TABLE III
ESTIMATION PERFORMANCES COMPARISON UNDER DIFFERENT WEIGHTS.

| Model | $\rho = 1$ | | | | $\rho = 0.1$ | | | | $\rho = 10$ | | | |
|-------|---------------------|----------------------------|------------------------------|----------------------------|---------------------|----------------------------|------------------------------|----------------------------|---------------------|----------------------------|------------------------------|----------------------------|
| | $\hat{\mathcal{L}}$ | \mathcal{L}^{acc} | $\mathcal{L}^{\text{huber}}$ | \mathcal{L}^{reg} | $\hat{\mathcal{L}}$ | \mathcal{L}^{acc} | $\mathcal{L}^{\text{huber}}$ | \mathcal{L}^{reg} | $\hat{\mathcal{L}}$ | \mathcal{L}^{acc} | $\mathcal{L}^{\text{huber}}$ | \mathcal{L}^{reg} |
| #1 | 0.01158 | 0.00168 | 0.00966 | 0.00024 | 0.01998 | 0.00070 | 0.01032 | 0.00268 | 0.07662 | 0.00204 | 0.00736 | 0.00010 |
| #2 | 0.10219 | 0.00184 | 0.09884 | 0.00151 | 0.11568 | 0.00133 | 0.09862 | 0.00380 | 1.00642 | 0.00242 | 0.09906 | 0.00134 |
| #3 | 0.10211 | 0.00182 | 0.09891 | 0.00138 | 0.12586 | 0.00215 | 0.10052 | 0.00386 | 1.02590 | 0.00555 | 0.10087 | 0.00117 |
| #4 | 0.21328 | 0.00003 | 0.16752 | 0.04573 | 0.20802 | 0.00008 | 0.16199 | 0.04526 | 2.25766 | 0.00011 | 0.17638 | 0.04938 |
| #5 | 0.20096 | 0.00003 | 0.15770 | 0.04299 | 0.21298 | 0.00002 | 0.16646 | 0.04637 | 2.18866 | 0.00004 | 0.17043 | 0.04843 |

during back propagation. This superiority is particularly pronounced in the results for the IEEE-9, IEEE-14 and IEEE-57 systems, where the resulting estimation residuals are only 0.00966, 0.00437 and 0.00736. The best performances of the other learning models are respectively 0.09884, 0.03221 and 0.03694, larger than 5 times of the residuals of Model #1. The results of regularization term from Model #1 are also the lowest. As for the MSE, the results of Model #1 are slightly lower than those of Model #2 and #3. Noted that, benchmark results from Gurobi actually only concern the minimization of physics loss, thereby having relatively higher MSE. The physics losses of Model #1 are comparable to the results of Gurobi, indicating the effectiveness of Opt – Layer in solving constrained optimization problems.

Besides, although conventional E2E learning Models #4 and #5 successfully achieve the lowest MSE, the physical constraints are not incorporated at all. Since these models are trained solely by regression accuracy, their physical losses are substantially higher than those of the other models using hybrid loss function, resulting in larger overall losses, especially on the IEEE-14 and IEEE-136 systems. These results illustrate that a statistically accurate solution is not necessarily a physically consistent one. Through homogenizing the KKT conditions at the optimal solution and utilizing the implicit function theorem to calculate the derivatives for backward propagation, the constraints of the RSE problem are strictly embedded into the framework. Then, all the solutions generated during the training process satisfy the constraints.

Compared to PINN that exogenously incorporating constraints violation as soft penalties, such a structure allows the NN to naturally achieve lower physical losses.

D. Performances Comparison Under Different Weights

To investigate the influence of the physical loss weight ρ on the estimation results, three scenarios on the IEEE 9-bus system are designed. Each scenario represents a different trade-off: a balanced approach with $\rho = 1$, an emphasis on accuracy with $\rho = 0.1$, and an emphasis on physical consistency with $\rho = 10$.

Table III compares the performances of the above five E2E learning models under these three scenarios. It is evident that regardless of the value of ρ , Model #1 consistently achieves the lowest physical losses, even in the accuracy-focused scenario ($\rho = 0.1$). The physical losses for all models are comparable under the balanced ($\rho = 1$) and accuracy-focused scenarios. When physical consistency is prioritized ($\rho = 10$), the physical losses of Model #1 decreases substantially. In contrast, Models #2 and #3 employing the hybrid loss function but lack the Opt – Layer, fail to exhibit a similarly significant physical losses reduction.

For a clearer comparative visualization, the results in Table III are scaled and plotted on a radar chart, as depicted in Fig. 3. Specifically, \mathcal{L}^{acc} and \mathcal{L}^{reg} values are multiplied by $1e5$, $\mathcal{L}^{\text{huber}}$ by $1e3$, and the base-10 logarithm is then applied to all metrics. It is obvious that, MSE is more sensitive to ρ . As ρ increases, the MSE also increases for all the models.

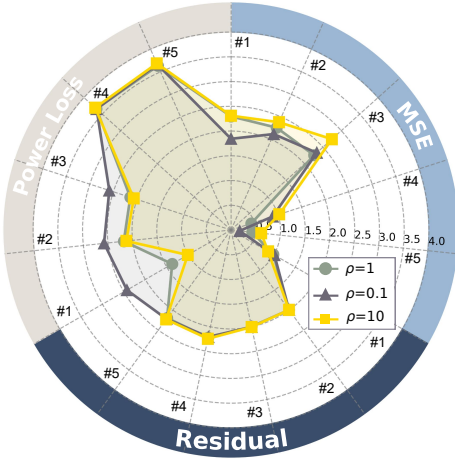


Fig. 3. Radar Chart of Estimation Performance Under Different Weights.

Model #1 outperforms all the other models in the estimation residuals under all three scenarios, and ρ has little impact on the residuals of the other four models. The power losses of Model #1 are sensitive to the setting of ρ , but are still the lowest. Models #4 and #5 achieve the lowest MSE across all settings for ρ , but they have the highest estimation residuals and active power losses.

VI. CONCLUSION

RSE is a critical tool for monitoring the operation states of smart grids considering the presence of outliers in measurements. Traditional E2E learning approaches for RSE prioritize regression accuracy while hard to ensure the physical consistency. To bridge this gap, this paper develops a novel E2E learning framework. The core innovation lies in the construction of a differentiable optimization layer Opt – Layer strictly embedded with KKT optimality conditions. To calculate the derivatives of global optimal solution with respect to problem parameters according to KKT conditions, convex relaxation techniques applicable to both radial and meshed power network topologies are utilized. Extensive simulations have validated the effectiveness of the proposed framework in boosting the overall estimation quality, including significantly lower physics loss and slightly higher estimation accuracy compared with classical E2E learning based approaches and PINN approaches.

The proposed framework offers distinct advantages and also presents avenues for future research. A primary strength is the rigorous optimality conditions embedding of Opt – Layer during backward propagation. This leads to the lowest physical losses compared to existing mainstream learning methods, as demonstrated in Section V. Furthermore, this architecture allows the NN to achieve enhanced richness of representation, maintaining a shallower structure. On the other hand, since the forward propagation involves repeatedly solving optimization problems, the offline training process could be computationally demanding.

Future work could include advanced acceleration techniques to reduce the computational burden of training. The research on dataset representativeness also worth in-depth investigation.

Moreover, extending the framework to a distributed architecture would enhance its scalability and suitability for modern power distribution networks characterized by the rapid growth of distributed renewable energy resources [37] [38].

APPENDIX A

CONDITIONS OF EXACT RELAXATION

The solution to the relaxed problem (P2) is guaranteed to be rank-one if the following conditions are satisfied [33]:

- 1) **Observability:** Voltage magnitude measurements V_i are available for all nodes. Active power flow measurements P_{ij} are available for a set of branches that forms at least one spanning tree of the power network.
- 2) **Operation condition:** The phase angle difference across any line is maintained within the range of -90° to 90° .

These conditions could be generally satisfied in modern power systems equipped with SCADA, operating under normal (i.e., non-heavily loaded) conditions [39].

APPENDIX B

PROOF OF COROLLARY 1

Recalling that, the total active power loss of a power system could be expressed as the algebraic addition of all nodal active power injection, namely $P_{loss} = \sum_{i \in \mathcal{N}} P_i$. According to AC power flow equations, the complex power injection at node i is calculated as:

$$S_i = V_i I_i^* = V_i (\sum_{j \in \mathcal{N}} Y_{ij} V_j)^* \quad (37)$$

whose real part denotes the active power injection at node i :

$$P_i = \text{Re}(S_i) = \text{Re}(\sum_{j \in \mathcal{N}} Y_{ij}^* V_i V_j^*) \quad (38)$$

Given the off-diagonal elements of the introduced auxiliary matrix $X_{ij} = V_i V_j (\cos \theta_{ij} + j \sin \theta_{ij}) = V_i V_j^*$, the total active power loss is therefore modeled as follows:

$$P_{loss} = \text{Re}(\sum_{i \in \mathcal{N}} \sum_{j \in \mathcal{N}} Y_{ij}^* X_{ij}) \quad (39)$$

We may also let $\Phi = (Y^*)^\top \mathbf{X}$, whose diagonal elements can be expressed as:

$$\Phi_{jj} = \sum_{i \in \mathcal{N}} (Y_{ji}^*)^\top X_{ij} = \sum_{i \in \mathcal{N}} Y_{ij}^* X_{ij} \quad (40)$$

Summing all off-diagonal elements, we have the trace of Φ :

$$\text{Tr}(\Phi) = \sum_{j \in \mathcal{N}} \Phi_{jj} = \sum_{i \in \mathcal{N}} \sum_{j \in \mathcal{N}} Y_{ij}^* X_{ij} \quad (41)$$

whose real part is exactly the total active power loss of the power system, namely:

$$P_{loss} = \text{Re}(\text{Tr}(\Phi)) = G_{ij} \text{Re}(X_{ij}) + B_{ij} \text{Im}(X_{ij}) \quad (42)$$

which is exactly the regularization term in the objective of (P2) and (P3). It is also a linear function of decision variables.

REFERENCES

- [1] A. Abur and A. G. Exposito, *Power system state estimation: theory and implementation*. CRC press, 2004.
- [2] G. Cheng, Y. Lin, A. Abur, A. Gómez-Expósito, and W. Wu, “A survey of power system state estimation using multiple data sources: Pmus, scada, ami, and beyond,” *IEEE Transactions on Smart Grid*, vol. 15, no. 1, pp. 1129–1151, 2023.

- [3] A. Minot, Y. M. Lu, and N. Li, "A distributed gauss-newton method for power system state estimation," *IEEE Transactions on Power Systems*, vol. 31, no. 5, pp. 3804–3815, 2015.
- [4] Z. Liu, P. Li, C. Wang, H. Yu, H. Ji, W. Xi, and J. Wu, "Robust state estimation of active distribution networks with multi-source measurements," *Journal of Modern Power Systems and Clean Energy*, vol. 11, no. 5, pp. 1540–1552, 2022.
- [5] J. J. Grainger, *Power system analysis*. McGraw-Hill, 1999.
- [6] J. Zhao, G. Zhang, K. Das, G. N. Korres, N. M. Manousakis, A. K. Sinha, and Z. He, "Power system real-time monitoring by using pmu-based robust state estimation method," *IEEE Transactions on Smart Grid*, vol. 7, no. 1, pp. 300–309, 2015.
- [7] Y. Wang, Y. Sun, and V. Dinavahi, "Robust forecasting-aided state estimation for power system against uncertainties," *IEEE Transactions on Power Systems*, vol. 35, no. 1, pp. 691–702, 2019.
- [8] R. C. Pires, A. S. Costa, and L. Mili, "Iteratively reweighted least-squares state estimation through givens rotations," *IEEE Transactions on Power Systems*, vol. 14, no. 4, pp. 1499–1507, 1999.
- [9] S. Zhong and A. Abur, "Auto tuning of measurement weights in wls state estimation," *IEEE Transactions on Power systems*, vol. 19, no. 4, pp. 2006–2013, 2004.
- [10] V. S. Patel, S. Chakrabarti, and A. Sharma, "A weighted deep neural network for processing measurements for state estimation," *IEEE Transactions on Industrial Informatics*, vol. 20, no. 3, pp. 3530–3538, 2023.
- [11] M. K. Celik and A. Abur, "A robust wlav state estimator using transformations," *IEEE Transactions on Power Systems*, vol. 7, no. 1, pp. 106–113, 2002.
- [12] M. Göl and A. Abur, "Lav based robust state estimation for systems measured by pmus," *IEEE Transactions on Smart Grid*, vol. 5, no. 4, pp. 1808–1814, 2014.
- [13] H. Wu, Z. Xu, J. Zhao, and S. Chai, "Gridtopo-gan for distribution system topology identification," *IEEE Transactions on Industrial Informatics*, vol. 19, no. 4, pp. 5356–5366, 2022.
- [14] B. Azimian, R. S. Biswas, S. Moshtagh, A. Pal, L. Tong, and G. Dasarathy, "State and topology estimation for unobservable distribution systems using deep neural networks," *IEEE Transactions on Instrumentation and Measurement*, vol. 71, pp. 1–14, 2022.
- [15] P. Donti, B. Amos, and J. Z. Kolter, "Task-based end-to-end model learning in stochastic optimization," *Advances in neural information processing systems*, vol. 30, 2017.
- [16] Y. Ding, X. Sun, W. Shi, J. Ruan, J. Chen, Y. Zhao, and Z. Xu, "Optimal distributed energy management for local energy community: A decision regret oriented smart predict and optimize approach," *IEEE Transactions on Industrial Informatics*, 2025.
- [17] S. Falas, M. Asprou, C. Konstantinou, and M. K. Michael, "Robust power system state estimation using physics-informed neural networks," *IEEE Transactions on Industrial Informatics*, 2025.
- [18] Q.-H. Ngo, B. L. Nguyen, T. V. Vu, J. Zhang, and T. Ngo, "Physics-informed graphical neural network for power system state estimation," *Applied Energy*, vol. 358, p. 122602, 2024.
- [19] A. S. Zamzam and N. D. Sidiropoulos, "Physics-aware neural networks for distribution system state estimation," *IEEE Transactions on Power Systems*, vol. 35, no. 6, pp. 4347–4356, 2020.
- [20] S. Boyd and L. Vandenberghe, *Convex optimization*. Cambridge university press, 2004.
- [21] B. Amos and J. Z. Kolter, "OptNet: Differentiable optimization as a layer in neural networks," in *Proceedings of the 34th International Conference on Machine Learning*, ser. Proceedings of Machine Learning Research, vol. 70. PMLR, 2017, pp. 136–145.
- [22] J. Zhu, Y. Xu, J. Wang, J. Watson, J. Song, and H. Sun, "Decision-centric uncertainty sets for storage arbitrage: Integrating estimation and optimization," *IEEE Transactions on Power Systems*, 2025.
- [23] Y. Jia, Y. Su, C. Wang, and Y. Wang, "Optnet-embedded data-driven approach for optimal power flow proxy," *IEEE Transactions on Industry Applications*, 2024.
- [24] R. Xie, L. Xu, C. Li, and X. Yu, "Neural-optimization integration for ac optimal power flow: A differentiable warm-start approach," *Cyber-Physical Energy Systems*, 2025.
- [25] L. Sang, Y. Xu, H. Long, and W. Wu, "Safety-aware semi-end-to-end coordinated decision model for voltage regulation in active distribution network," *IEEE Transactions on Smart Grid*, vol. 14, no. 3, pp. 1814–1826, 2022.
- [26] A. Agrawal, B. Amos, S. Barratt, S. Boyd, S. Diamond, and J. Z. Kolter, "Differentiable convex optimization layers," *Advances in neural information processing systems*, vol. 32, 2019.
- [27] Y. Chen, Y. Yao, and Y. Zhang, "A robust state estimation method based on socp for integrated electricity-heat system," *IEEE Transactions on Smart Grid*, vol. 12, no. 1, pp. 810–820, 2020.
- [28] H. G. Aghamolki, Z. Miao, and L. Fan, "Socp convex relaxation-based simultaneous state estimation and bad data identification," *arXiv preprint arXiv:1804.05130*, 2018.
- [29] H. Zhu and G. B. Giannakis, "Power system nonlinear state estimation using distributed semidefinite programming," *IEEE Journal of Selected Topics in Signal Processing*, vol. 8, no. 6, pp. 1039–1050, 2014.
- [30] L. Vandenberghe and S. Boyd, "Semidefinite programming," *SIAM review*, vol. 38, no. 1, pp. 49–95, 1996.
- [31] Y. Yao, X. Liu, D. Zhao, and Z. Li, "Distribution system state estimation: A semidefinite programming approach," *IEEE Transactions on Smart Grid*, vol. 10, no. 4, pp. 4369–4378, 2018.
- [32] Y. Lan, H. Zhu, and X. Guan, "Fast nonconvex sdp solvers for large-scale power system state estimation," *IEEE Transactions on Power Systems*, vol. 35, no. 3, pp. 2412–2421, 2019.
- [33] Y. Zhang, R. Madani, and J. Lavaei, "Conic relaxations for power system state estimation with line measurements," *IEEE Transactions on Control of Network Systems*, vol. 5, no. 3, pp. 1193–1205, 2017.
- [34] R. Singh, B. C. Pal, and R. Jabr, "Choice of estimator for distribution system state estimation," *IET generation, transmission & distribution*, vol. 3, no. 7, pp. 666–678, 2009.
- [35] J. Zhao, G. Zhang, Z. Y. Dong, and M. La Scala, "Robust forecasting aided power system state estimation considering state correlations," *IEEE Transactions on Smart Grid*, vol. 9, no. 4, pp. 2658–2666, 2016.
- [36] S. G. Krantz and H. R. Parks, *The implicit function theorem: history, theory, and applications*. Springer Science & Business Media, 2002.
- [37] V. Kekatos and G. B. Giannakis, "Distributed robust power system state estimation," *IEEE Transactions on Power Systems*, vol. 28, no. 2, pp. 1617–1626, 2012.
- [38] A. Butler and R. H. Kwon, "Efficient differentiable quadratic programming layers: an admm approach," *Computational Optimization and Applications*, vol. 84, no. 2, pp. 449–476, 2023.
- [39] G. N. Korres and N. M. Manousakis, "State estimation and bad data processing for systems including pmu and scada measurements," *Electric Power Systems Research*, vol. 81, no. 7, pp. 1514–1524, 2011.